A birefringent reflector from a 1D anisotropic photonic crystal

2009 J. Phys.: Condens. Matter 21 485401

(http://iopscience.iop.org/0953-8984/21/48/485401)

J. Phys.: Condens. Matter **21** (2009) 485401 (10pp) doi:10.1088/0953-8984/21/48/485401

A birefringent reflector from a 1D anisotropic photonic crystal

N Ouchani[1], D Bria[1,2], B Djafari Rouhani[2] and A Nougaoui[1]

[1] Laboratoire de Dynamique et d'Optique des Matériaux, Département de Physique, Faculté des Sciences, Université Mohamed Premier, 60000 Oujda, Morocco
[2] Institut d'Electronique, de Microélectronique et de Nanotechnologie (IEMN), UMR CNRS 8520, Université de Lille 1, 59655 Villeneuve d'Ascq, France

E-mail: noama03@yahoo.fr, bria@fso.ump.ma, bahram.djafari-rouhani@univ-lille1.fr and nougaoui@fso.ump.ma

Received 31 May 2009, in final form 22 September 2009
Published 30 October 2009
Online at stacks.iop.org/JPhysCM/21/485401

Abstract
We demonstrate theoretically that a one-dimensional anisotropic photonic crystal can exhibit an absolute photonic band gap in which the propagation of light is prohibited for all polarizations and for a given incidence plane. Our structure is formed by the combination of a simple finite superlattice, composed of two alternating birefringent biaxial layers, with a cladding layer. The latter is made of the same material as one of the layers constituting the perfect superlattice, but with different orientation and thickness. We discuss whether the birefringence of the layers has a significant impact on the reflection gap. We have found that for reasonable values of structure parameters an absolute band gap can be obtained. Green's function method is used to derive the necessary expressions for our calculation. The effect of different parameters, namely, the orientation of the layers, the filling fraction, etc, is investigated to achieve a birefringent reflector.

(Some figures in this article are in colour only in the electronic version)

1. Introduction

Over the past decade, much experimental and theoretical work has been devoted to the concept of photonic crystals, because of various optoelectronic applications [1–6]. These crystals possess a frequency band that imposes rigorous conditions on the propagation of electromagnetic waves in and out of the structure. Recently, great effort has been made in the design and manufacture of artificial microstructures possessing an absolute and complete three-dimensional (3D) photonic band gap [7, 8]. A complete photonic band gap requires that there is no allowed photon propagation state in a specified frequency for all directions of propagation and polarizations. So, for frequencies within the complete band gap, the structure exhibits total reflectivity for all incident angles. This phenomenon is known as omnidirectional reflection. Nevertheless, several technological difficulties restrict the fabrication of such small three-dimensional structures (of the order of 100 nm), especially for photonic crystals in the visible region. However, the complication associated with three-dimensional photonic crystals led to the investigation of one-dimensional periodic structures [9–15], which are easier to fabricate than 2D and 3D ones, but still offer unique possibilities for light control.

A one-dimensional (1D) photonic crystal, called an omnidirectional reflector, has many advantages over its metallic counterpart. A metallic reflector can reflect light over a wide range of frequencies for arbitrary incident angles. At infrared, optical or higher frequencies there are, however, considerable dissipative losses owing to absorption. Unlike metallic reflectors, multilayer dielectric reflectors can have an extremely low loss and a high reflectivity at certain frequency ranges. Recently, it has been shown that a multilayer dielectric reflector can have a high reflectivity over a broad range of frequencies at all incident angles if the refractive index and the thickness of the constituent dielectric layer are correctly chosen. This kind of omnidirectional dielectric reflector has been attracting a great deal of attention and potential applications have been proposed [3–6, 16]. Using an omnidirectional mirror of a periodic anisotropic stack, Abdulhalim [16] proposed a reflective polarization conversion Fabry–Perot resonator. This device is based on the polarization conversion phenomenon obtained near the edge of the band gap. The omnidirectional dielectric reflector can also be of use

in integrated optics, optical fiber telecommunications, vertical cavity surface emitting lasers (VCSEL), laser cavities, etc.

The main feature of all 1D photonic crystals is that the property of omnidirectional reflection can occur with a simple finite superlattice (SL), when the velocities of light in the substrates are higher than the characteristic velocities of the superlattice constituents. The limitation related to the choice of the substrate can be removed in different ways [11, 17–19]. First, by combining the superlattice with a cladding layer consisting of a material with a low optical index (or high velocity) that acts like a barrier for the propagation of light generated in the substrate. Second, by stacking together two different periodic multilayers so that the omnidirectional photonic band gap of the resulting structure is the union of band gaps of the two multilayers.

Most previous researches, have involved the use of a number of periodic and quasi-periodic structures based on alternating homogeneous isotropic layers of high and low refractive index to achieve an omnidirectional reflector. To the best of our knowledge, there have been a few recent works involving the use of an anisotropic stack to study the reflection property [20, 21]. Abdulhalim [20] was the first to report on omnidirectional reflection in birefringent periodic multilayers consisiting of Šolc filter type structures. This study is further analyzed by Cojocaru [21]. These authors demonstrated that a Šolc folded type anisotropic dielectric structure exhibits omnidirectional reflection at any polarization over a wide spectral range. This structure is built from alternating birefringent uniaxial layers of equal thickness that have the same principal refractive indices and different orientations of principal axes with respect to the laboratory axes. It is shown also in [22] that a periodic stack of alternating layers of a magneto-optic film and dielectric layer can act as an omnidirectional reflector.

In this paper we focus our attention on the study of the birefringent reflector formed by birefringent biaxial layers. We demonstrate theoretically that a 1D anisotropic photonic crystal can display an absolute photonic band gap for a given incidence plane. Our reflector is a cladded-superlattice structure, in which the cladding layer is formed by the same material as one of the layers constituting the superlattice but with different orientation and thickness. We discuss whether the birefringence of the layers enhances the performance of the device compared with its isotropic counterpart. Appropriate choices of the material and geometrical properties are discussed to realize a birefringent reflector.

Our paper is organized as follows, in section 2 we present the theoretical expression of the dispersion relation and the reflection and transmission coefficients in the framework of Green's function method. Section 3 shows the numerical results of our reflector. The effect of different parameters, namely, orientation of the layers, filling fraction, etc is investigated. The conclusions are presented in section 4.

2. Model and formalism

We depict in figure 1 the geometrical structure of a birefringent reflector. It is formed by a finite SL embedded between two semi-infinite isotropic substrates with a cap layer inserted between the SL and substrate. The unit cell of the structure is composed of two birefringent biaxial materials: $NaNO_2$ (material $i = 1$) and SbSI (material $i = 2$). The cap layer labeled as 0 is made by $NaNO_2$ with different orientations of the principal axes (x, y, z) of the crystal with respect to those in the superlattice layers. The orientation of the birefringent biaxial layer i with respect to the fixed (XYZ) coordinate system is characterized by the Euler angles [24, 25] θ_i, ϕ_i and ψ_i. The materials constituting the layers ($i = 0, 1, 2$) of the structure are assumed homogeneous and nonmagnetic, and are characterized by their thickness d_i and their principal refractive indices [26] $n_x^{(0,1)} = 1.344$, $n_y^{(0,1)} = 1.411$, $n_z^{(0,1)} = 1.651$ and $n_x^{(2)} = 2.7$, $n_y^{(2)} = 3.2$, $n_z^{(2)} = 3.8$. All the interfaces are taken to be parallel to the (XY) plane of a Cartesian (laboratory) coordinate system and the Z axis is along the normal to the interfaces. The period of the superlattice is $D = d_1 + d_2$.

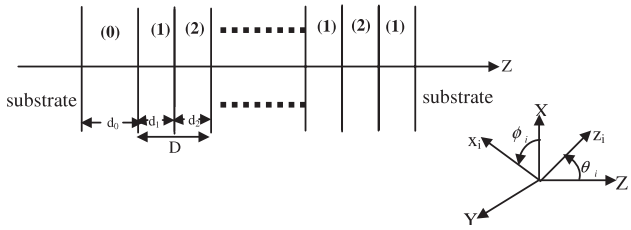

Figure 1. Finite anisotropic structure formed by two birefringent biaxial layers: $NaNO_2$ (material $i = 1$) and SbSI (material $i = 2$), with a cladding layer $NaNO_2$ (material $i = 0$). The structure is embedded between two semi-infinite isotopic media. The orientations of the layers are characterized by the polar angle θ_i and the azimuthal angle ϕ_i. d_i is the thickness of layer i, D is the period of the finite system.

Without any loss of generality, we assume an electromagnetic wave propagating in the (YZ) plane with the wavevector $\vec{K} = (0, q_Y, q_Z)$ and frequency ω. The different polarization directions q_Z of the electromagnetic wave are determined from the wave field equation in terms of the macroscopic electric field vector:

$$\vec{K} \wedge (\vec{K} \wedge \vec{E}) + q_0^2 \overleftrightarrow{\epsilon}\, \vec{E} = 0 \tag{1}$$

where $q_0 = \frac{\omega}{c}$, c is the velocity of light in a vacuum and $\overleftrightarrow{\epsilon}$ is the dielectric tensor, the expression for which is given in the appendix in the (XYZ) laboratory system. This equation can be rewritten as follows:

$$\begin{pmatrix} q_0^2\epsilon_{XX} - q_Y^2 - q_Z^2 & q_0^2\epsilon_{XY} & 0 \\ q_0^2\epsilon_{XY} & q_0^2\epsilon_{YY} - q_Z^2 & q_Z q_Y \\ 0 & q_Z q_Y & q_0^2\epsilon_{ZZ} - q_Y^2 \end{pmatrix} \times \begin{pmatrix} E_X \\ E_Y \\ E_Z \end{pmatrix} = \begin{pmatrix} 0 \\ 0 \\ 0 \end{pmatrix} \tag{2}$$

where E_X, E_Y, and E_Z are the components of the electric field in the laboratory axes. To have a nontrivial plane-wave solution, the determinant of the matrix in equation (2) must vanish. This yields four directions, two of them represent the forward propagating wave and the other two correspond to the backward propagating waves. Their expressions are

$$-q_Z^2 = \alpha_\pm^2 \tag{3}$$

where,

$$\alpha_{\pm}^2 = \frac{1}{2\epsilon_{ZZ}}\{[q_Y^2(\epsilon_{ZZ}+\epsilon_{YY}) - q_0^2\epsilon_{ZZ}(\epsilon_{XX}+\epsilon_{YY})] \pm [[k_Z^2\epsilon_{YY} - \epsilon_{ZZ}(q_Y^2 - q_0^2\epsilon_{XX})]^2 - 4q_0^2k_Z^2\epsilon_{ZZ}\epsilon_{XY}^2]^{\frac{1}{2}}\} \quad (4)$$

with $k_Z^2 = q_Y^2 - q_0^2\epsilon_{ZZ}$.

Using the appropriate Green's function, equation (2) is written as

$$\begin{pmatrix} q_0^2\epsilon_{XX} - q_Y^2 + \frac{\partial^2}{\partial Z^2} & q_0^2\epsilon_{XY} & 0 \\ q_0^2\epsilon_{XY} & q_0^2\epsilon_{YY} + \frac{\partial^2}{\partial Z^2} & -\mathrm{i}q_Y\frac{\partial}{\partial Z} \\ 0 & -\mathrm{i}q_Y\frac{\partial}{\partial Z} & q_0^2\epsilon_{ZZ} - q_Y^2 \end{pmatrix} \times \begin{pmatrix} G_{XX} & G_{XY} & G_{XZ} \\ G_{YX} & G_{YY} & G_{YZ} \\ G_{ZX} & G_{ZY} & G_{ZZ} \end{pmatrix} = \delta(Z - Z')\overleftrightarrow{I} \quad (5)$$

where $\overleftrightarrow{I}$ is a 3×3 unit matrix and G_{ij} are the elements of the bulk Green's function $G(Z, Z')$ determined by solving equation (5), whose elements are given in the appendix.

We would briefly recall the principle for building the Green function of the composite system. This will enable us to present the necessary formulae used in our calculation, namely, the dispersion relation and coefficients of reflection and transmission. Our calculation is based on the theory of interface response of continuous media. The object of this theory is to calculate the Green's function of a composite system containing a large number of interfaces that separate different homogeneous media. The knowledge of this Green's function enables us to obtain different physical properties of the system. In this theory, the Green's function of a composite system can be written as [27–29]

$$g(DD) = G(DD) + G(DM)\{[G(MM)]^{-1} \times g(MM)[G(MM)]^{-1} - [G(MM)]^{-1}\}G(MD) \quad (6)$$

where D and M are respectively the whole space and the space of the interfaces in the lamellar system. G is a block-diagonal matrix in which each block G_i corresponds to the bulk Green's function of the subsystem i (equation (5)). In our case, the composite material is composed of a SL built out of alternating slabs of materials i ($i = 1, 2$) with thickness d_i. In equation (6), all the matrix elements $g(DD)$ of the composite material can be obtained from the knowledge of the matrix elements $g(MM)$ of g in the interface space M. The $g(MM)$ is calculated by inverting the matrix $g^{-1}(MM)$ formed by a linear superposition of the surface matrix $g_{s_i}^{-1}(MM)$ of any independent film bounded by perfectly free interfaces with appropriate boundary conditions.

Before investigating the problem of layered materials, it is helpful to know the surface elements of the Green's function g_{s_i} of a slab of medium i. The principle step of the calculation of g_{s_i} is presented in the appendix. These surface elements can be written in the form of a 4×4 matrix $g_{s_i}(M_i, M_i)$, within the interface space $M_i \equiv \{\frac{-d_i}{2}, \frac{d_i}{2}\}$. The inverse of this matrix has the following form [30]:

$$[\overleftrightarrow{g}_{s_i}(M_i, M_i)]^{-1} = \begin{pmatrix} \overleftrightarrow{A}_i & \overleftrightarrow{B}_i \\ \overleftrightarrow{B}_i & \overleftrightarrow{A}_i \end{pmatrix} \quad (7)$$

where $\overleftrightarrow{A}_i$ and $\overleftrightarrow{B}_i$ are 2×2 matrices, whose elements are the forms:

$$\overleftrightarrow{A}_i = \begin{pmatrix} r_i & q_i \\ q_i & k_i \end{pmatrix} \quad \text{and} \quad \overleftrightarrow{B}_i = \begin{pmatrix} h_i & f_i \\ f_i & e_i \end{pmatrix} \quad (8)$$

where r_i, q_i, k_i, h_i, f_i, and e_i are defined in the appendix.

Within the total interface space of the infinite SL, the inverse of the matrix giving all the interface elements of the Green's function $g(MM)$ is an infinite tridiagonal matrix formed by linear juxtaposition of the elements $g_{s_i}^{-1}(M_i, M_i)$. We apply the Fourier transformation in the elementary cell of the tridiagonal matrix to obtain the following dispersion relation for the (YZ) incidence plane:

$$\alpha\cos^2(k_B D) + 2\beta\cos(k_B D) + \delta = 0 \quad (9)$$

where the elements α, β, and δ are defined as

$$\begin{aligned}
\alpha &= 4(e_2h_2 - f_2^2)(e_1h_1 - f_1^2)\\
\beta &= 2f_1f_2[f_1^2 + f_2^2 - (r_1+r_2)(k_1+k_2)]\\
&\quad + (f_2e_1 + f_1e_2)[2(q_1+q_2)(r_1+r_2) - h_1f_1 - h_2f_2]\\
&\quad + (f_2h_1 + f_1h_2)[2(q_1+q_2)(k_1+k_2) - e_1f_1 - e_2f_2]\\
&\quad + h_1h_2[e_1^2 + e_2^2 - (k_1+k_2)^2]\\
&\quad + e_1e_2[h_1^2 + h_2^2 - (r_1+r_2)^2]\\
&\quad - (q_1+q_2)^2[h_2e_1 + h_1e_2 + 2f_1f_2]\\
\delta &= [(r_1+r_2)(k_1+k_2) - (q_1+q_2)^2]^2\\
&\quad - [(r_1+r_2)e_1 - (q_1+q_2)f_1]^2 - [(r_1+r_2)e_2\\
&\quad - (q_1+q_2)f_2]^2 - [(q_1+q_2)f_1 - (k_1+k_2)h_1]^2\\
&\quad - [(q_1+q_2)f_2 - (k_1+k_2)h_2]^2 + [e_1h_1 - f_1^2]^2\\
&\quad + [e_1h_2 + e_2h_1]^2 + [e_2h_2 - f_2^2]^2\\
&\quad - 2(r_1+r_2)(k_1+k_2)(f_1^2 + f_2^2)\\
&\quad + 2(q_1+q_2)(r_1+r_2)\cdot(e_1f_1 + e_2f_2)\\
&\quad - 2(q_1+q_2)^2(h_1e_1 + h_2e_2)\\
&\quad + 2(q_1+q_2)(k_1+k_2)(h_1f_1 + h_2f_2)\\
&\quad + 4f_1f_2[f_1f_2 - h_2e_1 - h_1e_2] - 0.5\alpha.
\end{aligned}$$

Let us notice that the analytical expression of the dispersion relation of the anisotropic photonic crystal calculated in the framework of a Green's function method is simpler than using the 4×4 matrix approach (equation 7 in ref [31]). This method allowed the authors in [20, 22, 23] to calculate analytically the propagation matrix for one single layer in order to deduce numerically the dispersion relation for any anisotropic multilayered structure.

Within the theory of interface response function, the reflected and transmitted waves $u(D)$, resulting from a uniform plane wave $U(D)$ incident upon a plane boundary between two different media, are given by [27–29]

$$u(D) = U(D) + G(DM)\{[G(MM)]^{-1} \times g(MM)[G(MM)]^{-1} - [G(MM)]^{-1}\}U(M). \quad (10)$$

Let us mention that the incident wave, generated in the substrate s, can have two different polarizations, namely, transverse electric TE ($E \perp$ plane of incidence) or magnetic TM ($E \parallel$ plane of incidence). Each wave propagating inside

the anisotropic media generates two transmitted waves and two reflected waves with different polarizations. Let us call E_{iS} and E_{iP} the amplitudes of the S and P components of the incident field. Then, the amplitudes of the reflected and transmitted fields can be written as [30]

$$\vec{E}_{RS}(z) = r_{SS}\vec{E}_{iS}(z) + r_{SP}\vec{E}_{iP}(z) \tag{11}$$

$$\vec{E}_{TS}(z) = t_{SS}\vec{E}_{iS}(z) + t_{SP}\vec{E}_{iP}(z) \tag{12}$$

$$\vec{E}_{RP}(z) = r_{PS}\vec{E}_{iS}(z) + r_{PP}\vec{E}_{iP}(z) \tag{13}$$

$$\vec{E}_{TP}(z) = t_{PS}\vec{E}_{iS}(z) + t_{PP}\vec{E}_{iP}(z). \tag{14}$$

The expressions of r_{ij} and t_{ij} in these equations, with $i, j = S$ or P, are given in the appendix.

3. Discussion and numerical results

3.1. A semi-infinite superlattice in contact with an isotropic substrate

We consider a semi-infinite superlattice consisting of two alternating anisotropic media. As mentioned above (figure 1), the orientation of each birefringent biaxial layer with respect to the fixed (XYZ) coordinate system is characterized by the Euler angles $(\phi_i, \theta_i, \psi_i)$. When the principal axes of layers are parallel or perpendicular to the fixed axes, the transverse electric TE (S-mode) and transverse magnetic TM (P-mode) modes of an optical wave in a 1D photonic structure are decoupled [30, 31]. The two modes S and P are strongly coupled when the principal axes of the anisotropic media constituting the SL have an arbitrary orientation [30, 31]. In all the numerical results, we assumed $\psi = 0°$, $\theta = 0°$, or 90° and we take the azimuthal angle as a variable.

We display in figure 2, the projected band structure of a semi-infinite periodic multilayer. The band structure has been calculated using the analytical form of the dispersion equation derived for an infinite anisotropic superlattice (equation (9)). It is important to note that infinite and semi-infinite photonic crystals have the same band structure, the only difference is the existence of surfaces modes in the case of a semi-infinite structure. In this illustration, we suppose that the two layers 1, 2 are characterized with the following orientations $(\phi_1 = 0°, \theta_1 = 0°)$ and $(\phi_2 = 45°, \theta_2 = 90°)$. The thicknesses d_1 and d_2 of the layers are chosen such that $n_{z1}d_1 = n_{z2}d_2$. The dimensionless frequency $\Omega = \frac{\omega D}{2\pi c}$ and dimensionless wavevectors $K_{\parallel} = \frac{k_{\parallel} D}{2\pi}$ have been used in numerical illustrations, $k_{\parallel}$ is the wavevector parallel to the layers and c is the speed of light in vacuum. Depending on real or imaginary Bloch wavenumbers, an infinite periodic structure can support both propagating and evanescent Bloch waves. In figure 2, gray areas correspond to the propagating states, whereas white areas contain the evanescent states only and are usually referred to as photonic band gaps. One obvious feature of figure 2 is that there is no absolute gap, this means a gap existing for every value of the wavevector $k_{\parallel}$. The nonexistence of the absolute photonic band gap in one-dimensional photonic crystal is the cause of two factors. The first is that the edges of the directional photonic band gaps (photonic band gap

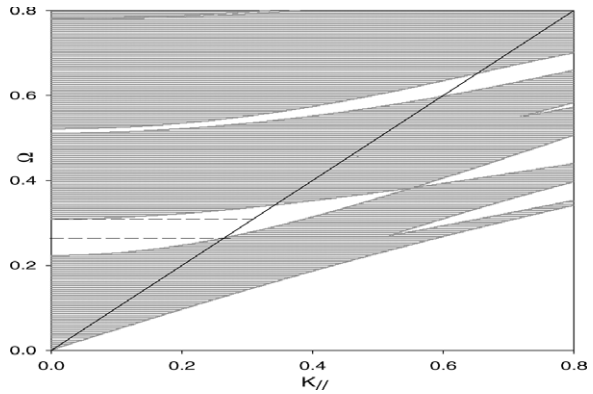

Figure 2. Projected photonic band structure of the ($NaNO_2$/SbSI) superlattice. The reduced frequency $\Omega = \frac{\omega D}{2\pi c}$ is presented as a function of the reduced wavevector $K_{\parallel} = \frac{k_{\parallel} D}{2\pi}$. The gray and white regions correspond to the pass bands and to the gaps of the superlattice, respectively. The azimuthal and polar angles (ϕ_i, θ_i) of the layers $NaNO_2$ and SbSI are assumed to be (0°, 0°) and (45°, 90°), respectively. The thicknesses d_1 and d_2 of the layers are chosen such that $n_{z1}d_1 = n_{z2}d_2$. The straight full line shows the light line of the vacuum. The area delimited by the two dashed lines and the vacuum light line represents the reflection gap.

at a certain direction) will shift to higher frequencies with the increase in incident angle, usually leading to the closure of the overall photonic band gap. The second is that the electromagnetic wave propagates without any reflection at the Brewster angle. However, the absence of an absolute photonic band gap does not mean that there is no total reflection. The criterion for the existence of total reflection is that there are no propagating modes that can couple the incident wave. We mentioned that the range of the reflection gap (RG) in figure 2 is marked by two dashed solid lines when the incident light is launched from a medium with a low index of refraction such as air ($n_s = 1$). When the frequency falls in this range, the wave cannot propagate inside the superlattice and will be reflected back. For decoupled modes, the RG for both TE and TM polarizations is defined by the edges of the upper photonic band gap at the grazing incidence and the lower photonic band gap at the normal incidence. The RG is always narrower and is closed up for a smaller refractive index of the ambient medium (n_s) for TM polarization than for TE one. The refractive index controls the width of RG with respect to the given parameters of the layers constituting the 1D photonic crystal. In figure 3, we study the evolution of the width of RG versus n_s. It is shown that the lower edge of the gaps shifts towards a higher frequency when the refraction index increases. Thus, the width of the gaps decreases till the reflection gap is closed up.

In order to achieve a structure with a wide RG, it is important to investigate the influence of the parameters characterizing the photonic crystal, namely, the filling fraction $\frac{d_2}{D}$ and the orientations of the axes of layers. We present in figures 4(a) and (b) a color map of the width $\Delta\Omega$ of the reflection gap as a function of both the azimuthal angle ϕ_i and the filling fraction. In these two illustrations, figures 4(a) and (b), we assume that the azimuthal angle ϕ_1 (ϕ_2) of the first (second) crystal layer $NaNO_2$ (SbSI) is zero and we take the azimuthal angle ϕ_2 (ϕ_1) of the second (first) crystal layer

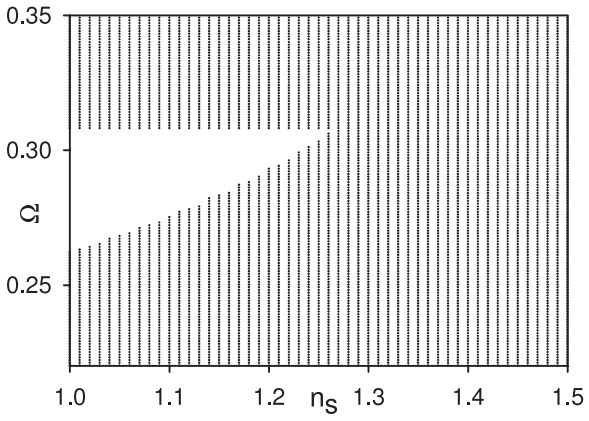

Figure 3. Variation of the frequency Ω of the reflection gap versus the refractive index of substrate n_s. The structural parameters are the same as in figure 2.

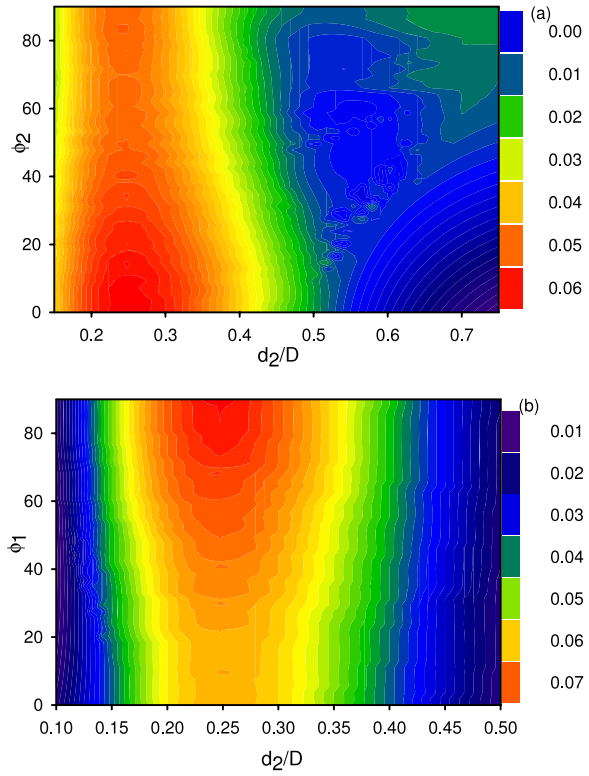

Figure 4. A color map of the width ΔΩ of the RG as a function of both the azimuthal angle ϕ_i and the filling fraction $\frac{d_2}{D}$. The polar angle and the thickness of the layers constituting the superlattice are the same as in figure 2. (a) Corresponds to the azimuthal angle $\phi_1 = 0°$ and (b) to $\phi_2 = 0°$.

SbSI ($NaNO_2$) as a variable. The red (black) and blue (gray) colors indicate, respectively, the high and low values of the width of RG. It can be noted that these structural parameters of anisotropic layers have an important effect on the bandwidth for RG. The maximum value of ΔΩ is obtained at a value of 0.25 of the filling fraction for both cases. In figure 4(a), ΔΩ reaches its maximum ($\Delta\Omega = 0.061$) when $0° \leqslant \phi_2 \leqslant 10°$ and in figure 4(b) the RG reaches a maximum value ($\Delta\Omega = 0.077$) around $\phi_1 = 90°$.

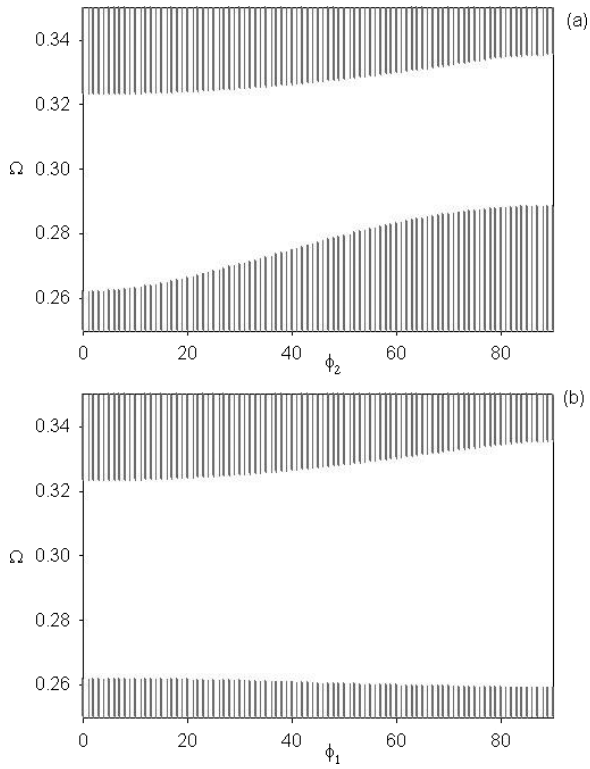

Figure 5. Variation of the frequency Ω of the RG as a function of the azimuthal angle ϕ_2 while $\phi_1 = 0°$ for curve (a) and ϕ_1 while $\phi_2 = 0°$ for curve (b). The filling fraction equals 0.25 and the polar angles θ_i of the layers have the same values as in figure 2.

To evaluate only the effect of the azimuthal angle ϕ on the width of the RG for this proper choice of film thickness, we present in figures 5(a) and (b) its width as a function of ϕ_1 and ϕ_2 for two layers, respectively. One can remark that the variation of bandwidth depends on the birefringence of the layer constituting the superlattice. In figure 5(a), the lower edge of the RG shifts to higher frequencies with the increase in azimuthal angle ϕ_2 of the strongly anisotropic layer SbSI, leading to the narrower RG. However, in figure 5(b), the width of the RG is rather larger when the angle ϕ_1 of the slightly biaxial layer $NaNO_2$ increases, because the lower edge of the RG shifts to lower frequencies when ϕ_1 increases. Thus, the birefringence of layers enhances the performance of the mirror compared with its isotropic counterpart by enlarging the spectral width of the band of reflection.

Nevertheless, if we illuminate the boundary of a semi-infinite superlattice from a substrate made of a material with high refractive index, the wave will be partially transmitted through the superlattice, and only partially reflected back, depending upon the incidence angle or the wavevector $k_{\|}$. The ability of the photonic crystal to behave like a perfect mirror imposes a limitation on the choice of substrate. In previous work [11, 17–19], the authors proposed two alternative solutions to overcome this difficulty. One solution would be to associate the superlattice with a cladding layer having high velocities of light (or lower indices of refraction) in order to create a barrier for the propagation of photonic waves. Another solution would consist of associating two or a few superlattices

chosen appropriately in such a way that the superposition of their band structures displays a complete photonic band gap. However, when the total number of periods of the mirror increases, the fabrication complexity increases.

In our paper we examine whether an anisotropic substrate can remove the limitation related to the choice of substrate. Thus, the anisotropic photonic crystal exhibits an absolute photonic band gap.

3.2. Semi-infinite superlattice in contact with an anisotropic substrate

The plane electromagnetic wave is considered to illuminate the boundary of a semi-infinite photonic crystal at an angle θ_i from a semi-infinite anisotropic homogeneous medium. The semi-infinite superlattice $NaNO_2$/SbSI is characterized by the parameters $(\phi_1, \theta_1, \phi_2, \theta_2, d_2)$, shown above, for a wide reflection gap: $(65°, 0°, 0°, 90°, 0.25)$. The anisotropic substrate is formed by the material $NaNO_2$ with a different orientation of its axes. In our study, we have taken the material $NaNO_2$ as a substrate, because the width of RG gradually increases with the increase of the azimuthal angle characterizing the orientation of the anisotropic crystal (figure 5(b)) unlike for the material SbSI (figure 5(a)). For particular cases, we investigate in figure 6 the effect of polar and azimuthal angles on the absolute RG. The photonic band structures shown in figures 6(a) and (b) correspond to $(\phi_0 = 0°, \theta_0 = 90°)$ and $(\phi_0 = 0°, \theta_0 = 0°)$ of the substrate, respectively. White and gray regions respectively represent the forbidden and allowed bands. The area between the two horizontal lines give the absolute RG. The effect of the polar angle on the presence of the Brewster window can clearly be seen in figure 6(b). The structure displays an absolute photonic band gap when the polar angle of the substrate is different from the polar angle of layers constituting the superlattice (figure 6(a)). However, the azimuthal angle cannot open the RG for both TE and TM polarizations for an identical polar angle of substrate and layers forming the photonic crystal (figure 6(b)).

In fact, the number of periods of the superlattice is finite in a real system, which is grown on a substrate and usually has a buffer layer. In experiments, the deposit of a superlattice on a substrate requires the existence of an intermediate layer (buffer layer) to avoid the problem of direct growth of the layers on a substrate. The objective of our work is to show the effect of the buffer layer in obtaining an absolute RG whatever the type of substrate. Indeed we have seen in figure 3 that with a substrate (incident medium) with low indices of refraction as compared to the indices in the superlattice constituents, it is possible to obtain an RG. However, it is not possible to obtain such an RG if the substrate is made of a material with high indices of refraction. Our purpose is to show that such an RG can again be obtained by adding a buffer layer with low indices of refraction at the entrance of the superlattice to play the role of a barrier. We investigate the structural parameters for the formation of the absolute photonic band gap in a cladded finite superlattice.

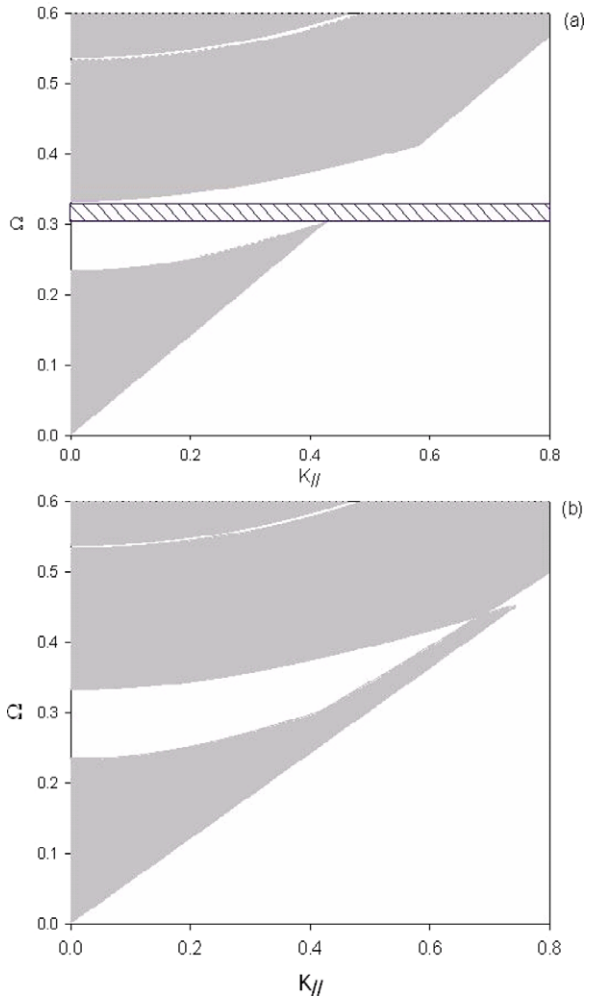

Figure 6. Projected band diagram of a semi-infinite anisotropic periodic multilayer. A substrate is made with the material $NaNO_2$, but with different orientations (ϕ_i, θ_i). Curves (a) and (b) correspond to $(0°, 90°)$ and $(0°, 0°)$, respectively. The other parameters of SL layers are mentioned in the text.

3.3. Cladded finite superlattice embedded between two substrates

The structure is formed with a finite $NaNO_2$/SbSI SL clad on one side by a biaxial layer $NaNO_2$ of thickness d_0, and embedded between two substrates made of an isotropic medium with high refractive index ($n_s = 4$). The finite system contains $N = 14$ layers of SbSI and $N + 1$ layers of $NaNO_2$. All layers of a cladded finite superlattice are characterized by the same parameters which optimize the formation of an absolute band gap as shown in section 3.2. In a finite superlattice structure, the transmission never reaches zero, but can decrease up to values close to zero in a certain range of frequency. Let us define the RG as a frequency interval in which the transmission intensity falls below a certain threshold whatever the incidence angle or the polarization of the wave. By fixing the threshold at 10^{-3}, we briefly discuss the existence and behavior of the RG as a function of the geometrical parameters involved in our structure, namely, the thickness d_0 of the $NaNO_2$, the azimuthal angle of a $NaNO_2$ layer, and

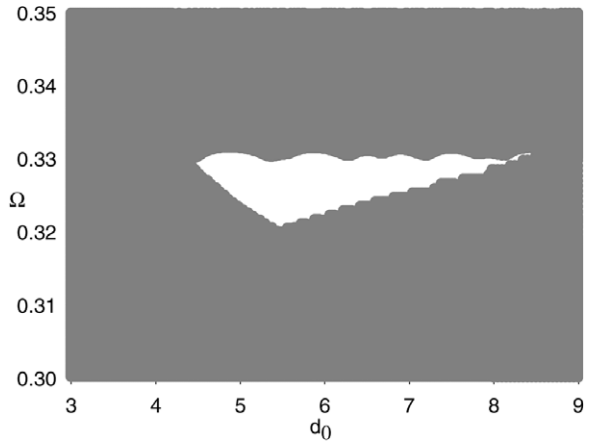

Figure 7. Dependence of the RG on the thickness d_0 of the cladding layer. the number of unit cells is $N = 14$. The transmission threshold is fixed at 10^{-3}.

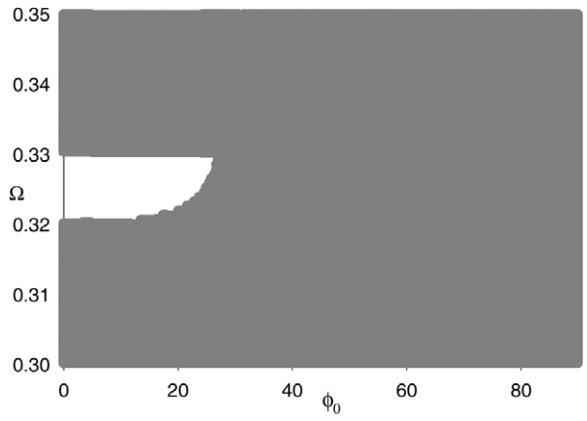

Figure 9. Dependence of the RG on the azimuthal angle ϕ_0 of the cladding layer. The number of unit cells is $N = 14$ and the thickness of the cladding layer is $d_0 = 5.4$. The transmission threshold is fixed at 10^{-3}.

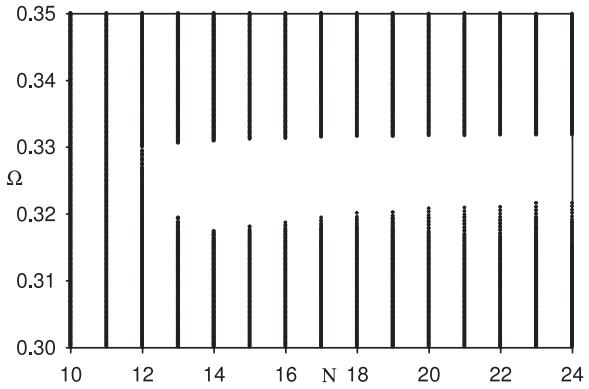

Figure 8. Dependence of the reflection gap on the number of unit cells N of the superlattice. The thickness of the cladding layer $d_0 = 5.4D$. The transmission threshold is fixed at 2×10^{-3}.

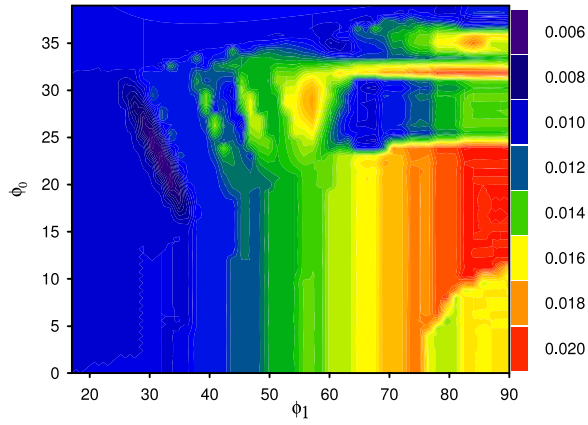

Figure 10. Color map of the width $\Delta\Omega$ of an absolute RG as a function of both the azimuthal angle ϕ_0 of the cladding layer and ϕ_1 of $NaNO_2$ layers of SL. The transmission threshold is fixed at 10^{-3}.

the number N of unit cells in the superlattice. In figure 7, we present the evolution of RG versus the thickness d_0. It appears that the bandwidth reaches its maximum value at approximately $d_0 = 5.4D$. By increasing the thickness of this layer, the RG is closed for d_0 greater than $8D$. To emphasize the formation of the RG, we study in figure 8, the influence of the number N of unit cells of the superlattice on the transmission power when $d_0 = 5.4D$, the other parameters being kept the same as in the above illustration. The absolute gap is presented by assuming that the transmission remains below the threshold of 2×10^{-3}. For $N \geqslant 13$, the RG appears and its width increases with N, but the higher N, the smaller the enlargement of the band gap. The width of the absolute gap reaches its maximum value when $N = 14$.

For the sake of completeness, we also present in figure 9, the effect of variation of the azimuthal angle ϕ_0 of a cladding layer $NaNO_2$. the figure shows a strong effect of the orientation of this layer on the existence of the RG. The absolute gap disappears when the angle ϕ_0 is greater than 25°. In the region, $0° \leqslant \phi_0 \leqslant 25°$, when the transverse electric and transverse magnetic polarizations are slightly coupled, a relatively large RG may be obtained. In order to optimize exactly the value of the width $\Delta\Omega$ of an absolute band gap, we present in figure 10 a color map of $\Delta\Omega$ as a function of both the azimuthal angles ϕ_0 and ϕ_1 of the cladding layer and the layers $NaNO_2$ in the superlattice, respectively. The red and blue colors indicate, respectively, the high and low values of the width of an absolute RG. The largest width $\Delta\Omega = 0.02$ is obtained for $10° \leqslant \phi_0 \leqslant 24°$ and $80° \leqslant \phi_1 \leqslant 90°$.

A detailed study of the disorder effect on the misalignment of layers is out of the scope of this paper. However, to check the robustness of the designed photonic crystal in terms of the orientation alignment of the layers in the structure, we start from the reference case of figure 9 and change the orientations of each of the two types of layers in the superlattice arbitrarily by plus or minus 5°. It should be remembered that figure 9 was obtained for the transmission through a finite superlattice when putting the threshold for the transmission at 10^{-3}. Now, by rotating the angle ϕ_1 by $+$ or $-5°$, the behaviors do not change significantly with respect to those in figure 9 (see figures 11(a) and (b)). However, by changing the angle ϕ_2 in the more birefringent SbSI layers by $+$ or $-5°$, the RG no longer survives when the threshold for transmission is fixed

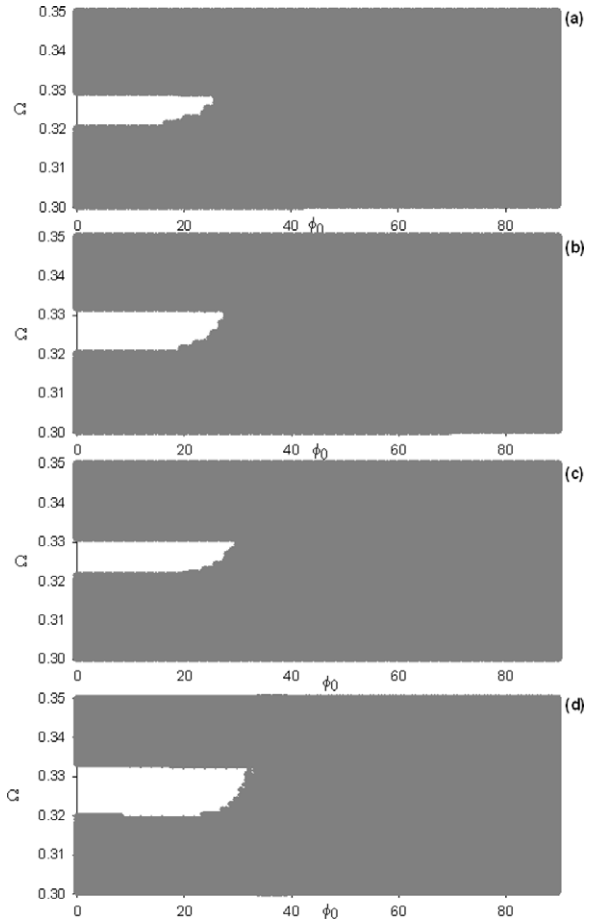

Figure 11. Same as in figure 9 but with the change of the orientations of the layers $NaNO_2$ by minus (a) or plus (b) 5° and the SbSI by plus (c) or minus (d) 5°. The transmission threshold is fixed for (a) and (b) at 10^{-3} and for (c) and (d) at 5×10^{-3}.

at 10^{-3}. By decreasing this threshold to 5×10^{-3}, one can see (figures 11(c) and (d)) that the RG appears again for some range of the angle ϕ_0. This RG can be widened if the threshold for the transmission is increased. One can understand that with the above change in the orientation of the SbSI layers, the cladding layer will become less efficient.

The isotropic omnidirectional reflector requires a cladding layer consisiting of a material having a low optical index that acts like a barrier for the propagation of light generated in the substrate, while this condition has some limitations due to the material's characteristics. However, our birefringent reflector requires a suitable choice of the orientations of the two crystals forming the structure to achieve an absolute photonic band gap regardless of the nature of the substrate.

4. Conclusions

In summary, we have demonstrated the existence of an absolute photonic band gap in a 1D anisotropic photonic crystal. This property can be achieved by the combination of a finite anisotropic superlattice with a cladding layer, which is made from the same material as one of the layers constituting the perfect superlattice, but with different orientation and thickness. A comprehensive study of the evolution of the gap characteristics versus structural parameters, namely, the orientation of the layers, the filling fraction, the thickness of the cladding layer, etc, has been presented. It is shown that the birefringence of the layers enhances the performance of the birefringent reflector as compared to the isotropic structure. The transmission coefficient and the dispersion curves presented in our results are based on analytical calculations of the Green's functions for optical waves in anisotropic multilayer structures.

Acknowledgments

D Bria acknowledges the hospitality of the Institut d'Electronique, de Microélectronique et de Nanotechnologie (IEMN), Université de Lille 1(France) where part of this work was carried out.

Appendix

(1) The bulk Green's function elements of an infinite anisotropic medium are given by

$$
\begin{aligned}
G_{XX}(Z,Z') &= -\frac{C}{2\alpha_-\alpha_+}[\alpha_- A_- \exp(-\alpha_+|Z-Z'|) \\
&\quad - \alpha_+ A_+ \exp(-\alpha_-|Z-Z'|)] \\
G_{YX}(Z,Z') &= -\frac{B}{D}\frac{C}{2\alpha_-\alpha_+}[\alpha_- \exp(-\alpha_+|Z-Z'|) \\
&\quad - \alpha_+ \exp(-\alpha_-|Z-Z'|)] \\
G_{ZX}(Z,Z') &= -\frac{\mathrm{i}q_Y C}{2}\frac{\epsilon_{XY}}{\epsilon_{ZZ}}[\exp(-\alpha_+|Z-Z'|) \\
&\quad - \exp(-\alpha_-|Z-Z'|)]\,\mathrm{sgn}(Z-Z') \\
G_{XY}(Z,Z') &= -\frac{B}{D}\frac{C}{2\alpha_-\alpha_+}[\alpha_- \exp(-\alpha_+|Z-Z'|) \\
&\quad - \alpha_+ \exp(-\alpha_-|Z-Z'|)] \\
G_{YY}(Z,Z') &= -\frac{C}{2\alpha_-\alpha_+ D}[\alpha_- A_+ \exp(-\alpha_+|Z-Z'|) \\
&\quad - \alpha_+ A_- \exp(-\alpha_-|Z-Z'|)] \\
G_{ZY}(Z,Z') &= -\frac{C}{2}\frac{\mathrm{i}q_Y}{q_0^2\epsilon_{ZZ}}[A_+ \exp(-\alpha_+|Z-Z'|) \\
&\quad - A_- \exp(-\alpha_-|Z-Z'|)]\,\mathrm{sgn}(Z-Z') \\
G_{XZ}(Z,Z') &= -\frac{\mathrm{i}q_Y C}{2}\frac{\epsilon_{XY}}{\epsilon_{ZZ}}[\exp(-\alpha_+|Z-Z'|) \\
&\quad - \exp(-\alpha_-|Z-Z'|)]\,\mathrm{sgn}(Z-Z') \\
G_{YZ}(Z,Z') &= -\frac{C}{2}\frac{\mathrm{i}q_Y}{q_0^2\epsilon_{ZZ}}[A_+ \exp(-\alpha_+|Z-Z'|) \\
&\quad - A_- \exp(-\alpha_-|Z-Z'|)]\,\mathrm{sgn}(Z-Z') \\
G_{ZZ}(Z,Z') &= \frac{1}{q_Y^2 - q_0^2\epsilon_{ZZ}}\left[\frac{1}{D}\delta(Z-Z')\right. \\
&\quad + \frac{C}{2}\frac{q_Y^2}{q_0^2\epsilon_{ZZ}}(\alpha_+ A_+ \exp(-\alpha_+|Z-Z'|) \\
&\quad \left. - \alpha_- A_- \exp(-\alpha_-|Z-Z'|))\right]
\end{aligned}
\tag{A.1}
$$

where

$A_{\pm} = (q_Y^2 - q_0^2\epsilon_{XX} - \alpha_{\pm}^2)$, $B = q_0^2\epsilon_{XY}$, $C = (\alpha_+^2 - \alpha_-^2)^{-1}$, $D = q_0^2\epsilon_{ZZ}(q_Y^2 - q_0^2\epsilon_{ZZ})^{-1}$, and $\delta(Z - Z')$ the Dirac delta function.

$q_0 = \frac{\omega}{c}$ is the vacuum wavevector, c is the velocity of light in vacuum, and ω is the frequency of the optical wave.

ϵ is the dielectric tensor, defined in the laboratory system (XYZ) by $\epsilon = A\epsilon_D A^{-1}$ where ϵ_D is the diagonal dielectric tensor such that $\epsilon_D = \mathrm{diag}(\epsilon_x, \epsilon_y, \epsilon_z)$ and A is the coordinate rotation matrix given by the following matrix for an arbitrary value of the azimuthal angle ϕ, the polar angle θ, and for $\psi = 0$ [26]:

$$\overleftrightarrow{A} = \begin{pmatrix} \cos(\phi) & -\cos(\theta)\sin(\phi) & \sin(\theta)\sin(\phi) \\ \sin(\phi) & \cos(\theta)\cos(\phi) & -\sin(\theta)\cos(\phi) \\ 0 & \sin(\theta) & \cos(\theta) \end{pmatrix}. \tag{A.2}$$

(2) The surface response function of the semi-infinite anisotropic medium.

The wave field equation in terms of the macroscopic electric field vector could be written for a medium limited by an opaque surface as

$$\Theta(Z)(q_0^2 \overleftrightarrow{\epsilon}\, \vec{E} - \vec{\nabla} \wedge (\vec{\nabla} \wedge \vec{E})) + \delta(z)\, \overleftrightarrow{V}(\vec{r})\vec{E} = 0 \tag{A.3}$$

where $\Theta(Z)$ is the Heaviside step function defined by

$$\Theta(Z) = \begin{cases} 1 & \text{si } Z \geqslant 0 \\ 0 & \text{si } Z < 0 \end{cases} \tag{A.4}$$

and $\overleftrightarrow{V}(\vec{r})$ is the operator of cleavage defined as a 3×3 matrix:

$$\overleftrightarrow{V}(\vec{r}) = \begin{pmatrix} \frac{\partial}{\partial Z} & 0 & 0 \\ 0 & \frac{\partial}{\partial Z} & -iq_Y \\ 0 & 0 & 0 \end{pmatrix}. \tag{A.5}$$

Using the theory of interface response function, the equation (A.3) is written as

$$\begin{pmatrix} q_0^2\epsilon_{XX} - q_Y^2 + \frac{\partial^2}{\partial Z^2} & q_0^2\epsilon_{XY} & 0 \\ q_0^2\epsilon_{XY} & q_0^2\epsilon_{YY} + \frac{\partial^2}{\partial Z^2} & -iq_Y\frac{\partial}{\partial Z} \\ 0 & -iq_Y\frac{\partial}{\partial Z} & q_0^2\epsilon_{ZZ} - q_Y^2 \end{pmatrix} \times \begin{pmatrix} g_{XX} & g_{XY} & g_{XZ} \\ g_{YX} & g_{YY} & g_{YZ} \\ g_{ZX} & g_{ZY} & g_{ZZ} \end{pmatrix} + \delta(Z) \begin{pmatrix} \frac{\partial}{\partial Z} & 0 & 0 \\ 0 & \frac{\partial}{\partial Z} & -iq_Y \\ 0 & 0 & 0 \end{pmatrix} \times \begin{pmatrix} g_{XX} & g_{XY} & g_{XZ} \\ g_{YX} & g_{YY} & g_{YZ} \\ g_{ZX} & g_{ZY} & g_{ZZ} \end{pmatrix} = \delta(Z - Z')\, \overleftrightarrow{I} \tag{A.6}$$

where $\overleftrightarrow{I}$ is a 3×3 unit matrix. In order to simplify the resolution of this equation, we envisage eliminating the third row and third column of the response function matrix with the help of the constitutive relations and work within the (XY) plane throughout. But this is not the only way to simplify the complex problem. One can choose to work in any plane and even start with equation (A.6) as such. The resulting cleavage operator in the (XY) plane takes the following form:

$$\overleftrightarrow{V}(Z) = \begin{pmatrix} \frac{\partial}{\partial Z} & 0 \\ 0 & -D\frac{\partial}{\partial Z} \end{pmatrix} \tag{A.7}$$

where D is defined as $D = q_0^2\epsilon_{ZZ}(q_Y^2 - q_0^2\epsilon_{ZZ})^{-1}$. The inverse of the surface response function of the semi-infinite anisotropic medium is given by [27–29]

$$\overleftrightarrow{g}_s^{-1}(0,0) = \overleftrightarrow{\Delta}_s(z,z')\overleftrightarrow{G}^{-1}(z,z')|_{z,z'=0} \tag{A.8}$$

where

$$\overleftrightarrow{\Delta}_s(0,0) = \overleftrightarrow{I} + \overleftrightarrow{V}(Z)\,\overleftrightarrow{G}(z,z')|_{z,z'=0} \tag{A.9}$$

where $\overleftrightarrow{G}^{-1}(0,0)$ is the inverse of the bulk response function in the (XY) plane taken at $(z, z' = 0)$. With the help of these equations, we can find the inverse of the surface response function of the semi-infinite anisotropic medium:

$$\overleftrightarrow{g}_s^{-1}(0,0) = \frac{1}{(\alpha_+ + \alpha_-)} \times \begin{pmatrix} -(k^2 + \alpha_+\alpha_-) & B \\ B & -D(k^2 - \alpha_+^2 - \alpha_-^2 - \alpha_+\alpha_-) \end{pmatrix} \tag{A.10}$$

where $k^2 = q_Y^2 - q_0^2\epsilon_{XX}$, B, and D are defined in equation (A.1) and $\alpha_{\pm}$ are defined in equation (4).

(3) The surface response function of the finite anisotropic medium.

The surface response function of a finite layer of an homogeneous medium i, extending in the region $\frac{-d_0}{2} \leqslant Z \leqslant \frac{d_0}{2}$ with free surfaces is given by [27–29]

$$\overleftrightarrow{g}_s^{-1}(M_i, M_i) = \overleftrightarrow{\Delta}_s(M_i, M_i)\overleftrightarrow{G}^{-1}(M_i, M_i). \tag{A.11}$$

$\overleftrightarrow{\Delta}_s(M_i, M_i)$ and $\overleftrightarrow{G}^{-1}(M_i, M_i)$ are defined within the interface space $M_i \equiv \{\frac{-d_i}{2}, \frac{d_i}{2}\}$. Then the $\overleftrightarrow{g}_s^{-1}(M_i, M_i)$ has the following form [30]:

$$[g_i(M_i, M_i)]^{-1} = \begin{pmatrix} A_i & B_i \\ B_i & A_i \end{pmatrix} \tag{A.12}$$

where A_i and B_i are 2×2 matrices, whose elements are the forms:

$$A_i = \begin{pmatrix} r_i & q_i \\ q_i & k_i \end{pmatrix} \quad \text{and} \quad B_i = \begin{pmatrix} h_i & f_i \\ f_i & e_i \end{pmatrix} \tag{A.13}$$

where r_i, q_i, k_i, h_i, f_i, and e_i are defined as

$$\begin{aligned} r_i &= -C_i[\alpha_{i+}A_{i-}\coth\theta_{i+} - \alpha_{i-}A_{i+}\coth\theta_{i-}] \\ q_i &= C_iB_i[\alpha_{i+}\coth\theta_{i+} - \alpha_{i-}\coth\theta_{i-}] \\ k_i &= -C_iD_i[\alpha_{i+}A_{i+}\coth\theta_{i+} - \alpha_{i-}A_{i-}\coth\theta_{i-}] \\ h_i &= C_i[\alpha_{i+}A_{i-}(\sinh\theta_{i+})^{-1} - \alpha_{i-}A_{i+}(\sinh\theta_{i-})^{-1}] \\ f_i &= C_iB_i[\alpha_{i-}(\sinh\theta_{i-})^{-1} - \alpha_{i+}(\sinh\theta_{i+})^{-1}] \\ e_i &= -C_iD_i[\alpha_{i-}A_{i-}(\sinh\theta_{i-})^{-1} - \alpha_{i+}A_{i+}(\sinh\theta_{i+})^{-1}] \end{aligned} \tag{A.14}$$

with

$$A_{i\pm} = (q_Y^2 - q_0^2\epsilon_{XX}^{(i)} - \alpha_{i\pm}^2), \qquad B_i = q_0^2\epsilon_{XY}^{(i)},$$

$$C_i = (\alpha_{i+}^2 - \alpha_{i-}^2)^{-1}, \qquad D_i = q_0^2 \epsilon_{ZZ}^{(i)} (q_Y^2 - q_0^2 \epsilon_{ZZ}^{(i)})^{-1}$$

$$\text{and} \qquad \theta_{i\pm} = \alpha_{i\pm} d_i.$$

(4) The expressions of the amplitude transmitted (t_{SS}, t_{PS}) and reflected (r_{SS}, r_{PS}) coefficients, when a pure (S) waves is incident, are of the form:

$$\begin{aligned} r_{SS} &= -(2\alpha d_{11} + 1) \qquad r_{PS} = -(2\alpha d_{21}) \frac{B_S}{B_P} \\ t_{SS} &= -(2\alpha d_{13}) \qquad t_{PS} = -(2\alpha d_{23}) \frac{B_S}{B_P} \end{aligned} \tag{A.15}$$

where $\alpha = (k_\parallel^2 - \frac{\omega^2 \epsilon_s}{c^2})^{\frac{1}{2}}$, $k_\parallel$ is the wavevector parallel to the (XY) interfaces, ω is the frequency of the optical wave, c the speed of light in a vacuum and ϵ_s the permittivity of the substrate.

$B_S = 1$ is the amplitude of the S wave and B_P, ($B_P = \frac{-i\alpha c}{\omega \sqrt{\epsilon_s}}$) is the amplitude of the P input wave.

d_{11}, d_{21}, d_{13}, and d_{23} are the elements of the truncated matrix of the finite system inserted between the two substrates presented in figure 1.

(5) The expressions of the amplitude transmitted (t_{PP}, t_{SP}) and reflected (r_{PP}, r_{SP}) coefficients when a pure TM (P) wave is incident are of the form:

$$\begin{aligned} r_{PP} &= \left(\frac{2q_0^2 \epsilon_s}{\alpha} d_{22} - 1\right) \qquad r_{SP} = \left(\frac{2q_0^2 \epsilon_s}{\alpha} d_{12}\right) \frac{B_P}{B_S} \\ t_{SP} &= \left(\frac{2q_0^2 \epsilon_s}{\alpha} d_{14}\right) \frac{B_P}{B_S} \qquad t_{PP} = \left(\frac{2q_0^2 \epsilon_s}{\alpha} d_{24}\right) \end{aligned} \tag{A.16}$$

as the same d_{12}, d_{22}, d_{14}, and d_{24} are the elements of the truncated matrix of the finite system.

We note here that the total reflectivities for the P and S modes are

$$R_P \equiv R_{PP} + R_{SP} = |r_{PP}|^2 + |r_{SP}|^2 \tag{A.17}$$

$$R_S \equiv R_{SS} + R_{PS} = |r_{SS}|^2 + |r_{PS}|^2 \tag{A.18}$$

and the total transmission for the P and S modes have the following expressions:

$$T_P \equiv T_{PP} + T_{SP} = |t_{PP}|^2 + |t_{SP}|^2 \tag{A.19}$$

$$T_S \equiv T_{SS} + T_{PS} = |t_{SS}|^2 + |t_{PS}|^2. \tag{A.20}$$

References

[1] Yablonovitch E 1987 *Phys. Rev. Lett.* **58** 2059–62
[2] John S 1987 *Phys. Rev. Lett.* **58** 2486–89
[3] Kim S H and Hwangbo C K 2002 *J. Appl. Opt.* **41** 3187–92
[4] Lo S S *et al* 2004 *Opt. Express* **12** 6589–93
[5] Lusk D and Placido F 2005 *Thin Solid Films* **492** 226–231
[6] Liu K *et al* 2006 *Appl. Phys.* B **82** 391–3
[7] Guida G *et al* 2003 *Prog. Electromagn. Res.* **41** 1–20
[8] Maka T *et al* 2003 *Prog. Electromagn. Res.* **41** 307–35
[9] Fink Y *et al* 1998 *Science* **282** 1679–82
[10] Winn J N *et al* 1998 *Opt. Lett.* **23** 1573–75
[11] Bria D *et al* 2002 *J. Appl. Phys.* **91** 2569–72
[12] Lee H Y and Yao T 2003 *J. Appl. Phys.* **93** 819–30
[13] Yonte T *et al* 2004 *J. Opt. A: Pure Appl. Opt.* **6** 127–31
[14] Wu C J 2006 *J. Electromagn. Waves Appl.* **19** 1991–96
[15] Aissaoui M *et al* 2006 *Prog. Electromagn. Res.* **59** 69–83
[16] Abdulhalim I 2003 *Opt. Commun.* **215** 225–30
[17] Han P and Wang H 2005 *J. Opt. Soc. Am.* B **22** 1571–75
[18] Wang X *et al* 2002 *Appl. Phys. Lett.* **80** 4291–3
[19] Xifré Pérez E *et al* 2005 *J. Appl. Phys.* **97** 064503-1–5
[20] Abdulhalim I 2000 *Opt. Commun.* **174** 43–50
[21] Cojocaru E 2000 *Appl. Opt.* **39** 4641
[22] Abdulhalim I 2000 *J. Opt. A: Pure Appl. Opt.* **2** 557–64
[23] Abdulhalim I 1999 *J. Opt. A: Pure Appl. Opt.* **1** 646–53
[24] Goldstein H 1957 *Classical Mechanics* (Reading, MA: Addison-Wesley) pp 107–9
[25] Landry G D and Maldonado T A 1995 *J. Opt. Soc. Am.* A **12** 2048
[26] Yeh P 1988 *Optical Waves in Layered Media* (*Wiley Series in Pure and Applied Optics*) (New York: Wiley) pp 201–53
[27] Dobrzynski L 1987 *Surf. Sci.* **180** 489
[28] Dobrzynski L 1990 *Surf. Sci.* **11** 139
[29] Dobrzynski L and Puszkarski H 1993 *J. Phys.: Condens. Matter* **5** 139
[30] Ouchani N *et al* 2007 *J. Opt. Soc. Am.* A **24** 2710–18
[31] Ouchani N *et al* 2006 *Sol. Cells* **90** 1445–57